Journal of Geophysical Research: Atmospheres

RESEARCH ARTICLE
10.1029/2018JD029178

Cold Electron Runaway Below the Friction Curve

G. Diniz[1,2], C. Rutjes[2], U. Ebert[2,3], and I. S. Ferreira[1]

[1]Instituto de Física, Universidade de Brasília, Brasília, Brazil, [2]Centrum Wiskunde & Informatica, Amsterdam, The Netherlands, [3]Department of Applied Physics, Eindhoven University of Technology, Eindhoven, The Netherlands

Key Points:
- We evaluate the stationary sub-keV electron energy distribution in air and nitrogen, in different electric fields
- Friction is not a systematic approximation for the energy loss of nonrelativistic electrons
- Cold electrons can accelerate to above 1-keV energy in electric fields close to 3 MV/m, well below the so-called runaway threshold

Correspondence to:
U. Ebert,
ute.ebert@cwi.nl

Citation:
Diniz, G. S., Rutjes, C., Ebert, U., & Ferreira, I. S. (2019). Cold electron runaway below the friction curve. *Journal of Geophysical Research: Atmospheres*, *124*, 189–198. https://doi.org/10.1029/2018JD029178

Received 14 JUN 2018
Accepted 3 DEC 2018
Accepted article online 7 DEC 2018
Published online 15 JAN 2019

Abstract Cold electron runaway means that free electrons in gases are accelerated by electric fields from eV energies to energies above tens of keV where they can be accelerated further. To run away, the electrons need to overcome a barrier at intermediate energies where they can lose much energy in collisions. When they have reached the runaway regime, they can produce high-energy radiation by bremsstrahlung that can be detected as (terrestrial) gamma ray flashes. When can thermal electrons from active discharges like streamers and leaders reach the runaway regime? The deterministic approach to this question is based on an energy-dependent electron friction that has to be overcome by electric acceleration. Taking the stochastic nature of the electron molecule collisions into account, we find (1) that the classical friction curve in the energy regime up to 1 keV does not characterize the mean electron energy, but rather, it seems to approximate the upper limit of the electron energy distribution and (2) that electrons can "tunnel" through the barrier when the field is close to 3 MV/m, below the so-called cold runaway threshold (or critical field) of approximately 26 MV/m in air at standard temperature and pressure. (3) This is only true in the bulk perspective where the electron liberation and attachment in a given electric field is taken into account in the continuously refreshing electron ensemble. In a flux simulation that follows individual electrons as long as they are free, electron attachment reduces electron runaway very strongly in air, differently to what we observe in nitrogen.

1. Introduction

1.1. High-Energy Atmospheric Physics and Electron Runaway

Active thunderstorms by now are well known to emit terrestrial gamma ray flashes (Briggs et al., 2011; Fishman et al., 1994; Østgaard et al., 2008) and gamma ray glows (Adachi et al., 2008; Chilingarian et al., 2010, 2011; Tsuchiya et al., 2007), and these gamma rays in turn create further particle species like electron positron beams (Briggs et al., 2011), neutrons (Babich et al., 2010; Bowers et al., 2017), terrestrial gamma ray flash afterglows (Enoto et al., 2017; Rutjes et al., 2017), and radioactive decay products of photonuclear reactions (Enoto et al., 2017). The gamma rays are due to the bremsstrahlung when high-energy electrons collide with air molecules. The whole chain of particle creation in high-energy atmospheric physics therefore starts with these high-energy electrons.

There are two basically different types of high-energy electron sources in the atmosphere. The first type of sources are cosmic particles or radioactive decay, where the primary particles already have high energy. Cosmic particles impinge with high energy onto our atmosphere and create showers of more elementary particles and then secondary collision products. If the primary energy is as high as 10^{15} to 10^{17} eV, extensive air showers can create substantial densities of secondary particles that can play a role in lightning inception (Dubinova et al., 2015). Air showers can be enhanced by high electric fields in thunderstorms, creating relativistic runaway electron avalanches (Babich et al., 2005; Dwyer, 2007; Dwyer et al., 2008). Radioactive decay of atmospheric components is another direct source of high-energy particles (Enoto et al., 2017). The second type of sources are low-energy electrons (with energies in the eV range) that are accelerated in the fields of electric discharges like streamers or leaders into the so-called runaway regime where they can keep accelerating when the acceleration in a local electric field is larger than the energy losses due to collisions with air molecules. To reach this regime, they have to pass through some intermediate energy regime where the dynamic friction due to collisions is larger. The present paper deals with this runaway process and the likelihood to pass through the friction barrier at intermediate energies toward runaway.

Table 1
List of the Electron Collisions With N_2 (left) and O_2 (right) Included in the Simulations

N_2 collisions			O_2 collisions		
Result	Collision type With N_2	Energy loss (eV)	Result	Collision type With O_2	Energy loss (eV)
N_2	Elastic	0	O_2	Elastic	0
N_2(rot)	Excitation	0.02	O_2(rot)	Excitation	0.02
N_2(v1res)	Excitation	0.29	O_2(v1)	Excitation	0.19
N_2(v1)	Excitation	0.291	O_2(v1res)	Excitation	0.19
N_2(v2)	Excitation	0.59	O_2(v2)	Excitation	0.38
N_2(v3)	Excitation	0.88	O_2(v2res)	Excitation	0.38
N_2(v4)	Excitation	1.17	O_2(v3)	Excitation	0.57
N_2(v5)	Excitation	1.47	O_2(v4)	Excitation	0.75
N_2(v6)	Excitation	1.76	O_2(a1)	Excitation	0.977
N_2(v7)	Excitation	2.06	O_2(b1)	Excitation	1.627
N_2(v8)	Excitation	2.35	O_2(4.5eV)	Excitation	4.5
N_2(A3,v0-4)	Excitation	6.17	O_2(6.0eV)	Excitation	6
N_2(A3,v5-9)	Excitation	7	O_2(8.4eV)	Excitation	8.4
N_2(B3)	Excitation	7.35	O_2(9.97eV)	Excitation	9.97
N_2(W3)	Excitation	7.36	O_2^+	Ionization	12.06 (Threshold energy)
N_2(A3,v10-)	Excitation	7.8	O_2^-	3-body attach.	—
N_2(B'3)	Excitation	8.16	O^-+O	Dissoc. attach.	—
N_2(a'1)	Excitation	8.4	—	—	—
N_2(a1)	Excitation	8.55	—	—	—
N_2(w1)	Excitation	8.89	—	—	—
N_2(C3)	Excitation	11.03	—	—	—
N_2(E3)	Excitation	11.87	—	—	—
N_2(a''1)	Excitation	12.25	—	—	—
N_2(SUM)	Excitation	13	—	—	—
N_2^+	Ionization	15.6 (Threshold energy)	—	—	—

Note. Different excitation types of the molecules are indicated as rot for rotations, v for vibrations, and all other symbols refer to electronic excitations. SUM is the sum over all singlet states. All cross section data are retrieved from the lxcat databank and refer to Phelps' compilation of measurements.

1.2. The Concept of the Friction Curve

Electron runaway was first proposed by Wilson (1924) who suggested that thunderstorms could generate strong enough electric fields for electrons to continuously gain more energy than they lose through collisions with air molecules. This concept was further elaborated and quantified by Gurevich et al. (1992) who argued that the minimum of dynamic friction is at about 1-MeV electron energy in atmospheric air and that an electric field above the threshold of 0.3 MV/m at standard temperature and pressure would maintain electron runaway at these energies. As discussed by Dwyer (2004), this dynamic friction curve for electrons with energies between 10 eV and 1 GeV can also be found in a report of the International Commission on Radiation Units and Measurements (ICRU) (1984). This is because dynamic friction acting on a particle is a common concept in high-energy physics. For example, a relativistic electron (with energy much above 1 MeV) on its path through matter loses energy mostly by creating many low-energy particles while it essentially keeps its original direction; so it effectively loses energy continuously and experiences some friction force, known as continuous slowing down approximation (CSDA), and it can be clearly distinguished by its high energy from the many liberated electrons in the electron volt regime. As discussed by Rutjes et al. (2016), this approximation is improved in some high-energy codes by including the generation of all secondary particles below an energy threshold ε_{cut} into an effective friction force acting in the primary particle, while collisions where the primary particle loses more energy are treated explicitly and stochastically. In nuclear physics where one is interested in the thickness of some material needed to shield some particle radiation, the friction on the energetic particle is also called the stopping power of the material it penetrates.

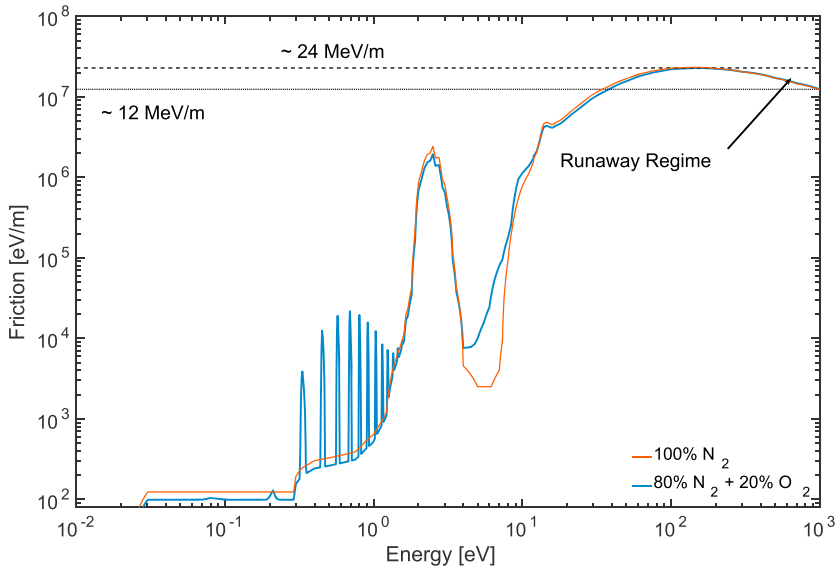

Figure 1. The friction curve as function of electron energy in the range from 0.01 eV to 1 keV for artificial air (which is a mixture of 80% nitrogen with 20% oxygen, blue curve) and for pure nitrogen (red curve), calculated according to the definition of Moss et al. (2006) that is reproduced in equations (1) and (2). Both curves are calculated with the processes listed in Table 1 and for a density defined by 273 K and 1 bar. The electric forces on electrons in electric fields of 12 and 24 MV/m are indicated by horizontal dotted and dashed lines, respectively.

While the friction concept is well based in high-energy physics, Moss et al. (2006) have applied the concept to low-energy electrons in the eV range as well, and, for example, Colman et al. (2010) and Chanrion et al. (2016) use the same concept. Moss et al. (2006) define the dynamic friction force $F_D(\epsilon)$ of an electron with energy ϵ through the equation

$$F_D(\epsilon) = \sum_{i,j} N_i \, \sigma_{i,j}(\epsilon) \, \delta\epsilon_{i,j}, \tag{1}$$

where N_i is the partial density of each air component i (nitrogen, oxygen, argon, etc.), $\sigma_{i,j}$ are the cross sections for an electron collision with a molecule of type i and collision type j (see Table 1), and $\delta\epsilon_{i,j}$ is the energy loss of the electron in the specific collision type. (Here we correct some notation error of the original paper of Moss et al. (2006), as one needs to sum over two indices, one for the molecule species, and one for the collision types.) For an ionizing collision, the energy loss is the function $\delta\epsilon_{i,\mathrm{ion}}(\epsilon)$ of the incident electron with energy ϵ is the ionization energy $\epsilon_{i,\mathrm{ion}}$ plus the kinetic energy of the liberated second electron. In this case the average energy loss is calculated as

$$\delta\epsilon_{i,\mathrm{ion}}(\epsilon) = \epsilon_{i,\mathrm{ion}} + \frac{\bar{\epsilon}}{2\arctan\frac{\epsilon-\epsilon_{\mathrm{ion}}}{2\bar{\epsilon}}} \ln\left[1+\left(\frac{\epsilon-\epsilon_{\mathrm{ion}}}{2\bar{\epsilon}}\right)^2\right], \tag{2}$$

where we used the empirical fit of Opal et al. (1971) with the constants $\bar{\epsilon} = 13.0$ eV for nitrogen and 17.5 eV for oxygen, and where we averaged over the energy distribution between the two outgoing electrons. Attachment cannot be taken into account in equation (1), as an attaching electron does not lose energy but rather completely disappears from the ensemble. Also, the second electron created in an impact ionization event cannot be incorporated into a friction force. In this sense, the friction concept is a flux concept that characterizes the behavior of individual particles but does not take the dynamical change of the particle ensemble into account.

The friction curve as defined above is shown in Figure 1 as a function of electron energy. Results for artificial air and for pure nitrogen at 273 K and 1 bar are shown. For the lowest energies, there are only rotationally excited states that cause little friction. The peaks in the range from 0.3 to 1 eV are due to the vibrational states of oxygen in air and absent in pure nitrogen. The electronic excitations above 1 eV create a local maximum of the friction at about 2.5 eV and are quite similar in air and in nitrogen. Also, the global maximum of the friction at about 200 eV is quite similar for the two gases. Beyond 200 eV the friction decreases toward the runaway regime.

1.3. Value and Validity of the Friction Curve in Different Energy Regimes

Moss et al. (2006) interpret their friction force by direct comparison with the electric force. Thus, the net force on an electron is approximated as the electric force minus the friction force. This interpretation leads to the notion of equilibrium points, where the net force of field acceleration and friction vanishes. These equilibrium points can be dynamically stable or unstable. When the friction increases with increasing electron energy, the electron will be driven back to a stable equilibrium point, and one would therefore expect that this point characterizes the mean electron energy in the given electric field. On the other hand, if the friction decreases for increasing electron energy, the electron will move further away from the equilibrium point, and the point is unstable.

While this interpretation is correct for high-energy electrons as they slow down almost continuously along a rather straight path as discussed above, it gives only a qualitative insight for electrons in the eV range and can lead to erroneous conclusions. This is the topic of the present paper. The major shortcomings of the deterministic friction approach in the electron volt regime are the following:

A. For a direct comparison between electric and friction forces, they need to be aligned, which is often not the case, as we exemplify below. The friction acts along any electron path, but electric acceleration acts only along the component of the path aligned with the electric field.
B. In particular, there is no energy loss related to elastic scattering, but the elastic scattering plays an important role in changing the propagation direction of the electrons and hence the energy gain from the electric field. This effect is ignored in equation (1).
C. The collisions are discrete and stochastic; therefore, there is no continuous energy loss, but rather, there are discrete moments of time at which the electron loses a random amount of energy and attains a new random propagation direction.
D. The deterministic friction approach cannot account for electron attachment to oxygen or other electronegative gas components or for electron multiplication by impact ionization. In this sense, it is a flux quantity, characterizing the evolution of an ensemble with a fixed number of electrons. We will see that attachment has an important effect in a flux ensemble when comparing air with pure nitrogen. However, we will show that this effect is suppressed in a bulk ensemble where the electron number is changing continuously.

Points A and B are well explored by Chanrion et al. (2016) and Skeltved et al. (2014).

Point C makes it possible for electrons to enter the runaway regime in electric fields below the maximum of the friction curve; since the energy gain is continuous and the energy loss is stochastic, there is a chance for the electrons to gain enough energy between collisions to reach an energy region where the friction decreases. This possibility was already observed by Li et al. (2009). We call this effect *tunneling through the friction curve*.

Point D is here analyzed further, since the friction equation (Bakhov et al., 2000; Chanrion et al., 2014, 2016; Moss et al., 2006) cannot include electron attachment or liberation. As said above, based on the similarity of the friction curves for pure nitrogen and for artificial air shown in Figure 1, one would expect similar runaway probabilities in both gases, but in a flux ensemble this is not seen.

1.4. This Work

We have analyzed the electron motion through air and pure nitrogen in a range of electric fields with a focus on the stochasticity of the collisions. To do so, we use a Monte Carlo approach with a previously developed code to study the equilibrium or steady state between electric and friction forces in an electron ensemble, exposed to constant electric fields in the range from 1 kV/m to 35 MV/m. We have also simulated the random motion of electrons starting with an energy of 200 eV in electric fields of 16 to 34 MV/m and their chance to run away.

2. Methodology

2.1. Software Framework

We have simulated electrons in air or nitrogen with the particle-in-cell (PIC) Monte Carlo code particle_core that is described in (Teunissen & Ebert, 2016) and available on https://github.com/jannisteunissen/particle_core. The code follows the electron motion in a given electric field and their collisions with air molecules, where collision time and type are determined by a Monte Carlo procedure; hence, the gas molecules are included as a random background of fixed density. The original code **particle_core** uses isotropic scattering of the electrons after collisions, which is appropriate for electron energies up to the

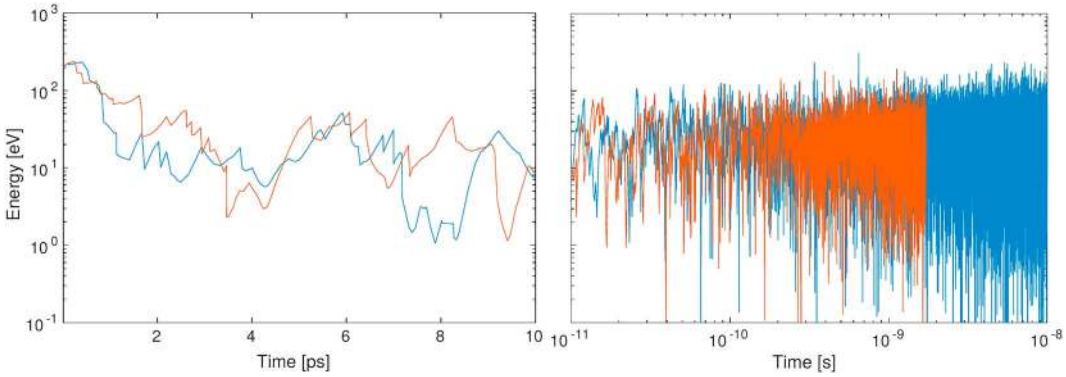

Figure 2. Statistical behavior of the electron energies in air in the flux simulation: energy fluctuations of two electrons (red and blue) in a 26-MV/m electric field as a function of time; the left panel shows the time from 0 to 10 ps on linear scale, the right panel from 10 ps to 10 ns on logarithmic scale.

order of 20 eV, and the range of validity can be stretched by renormalizing the cross sections; this is typically done for the cross sections on the lxcat.net database (https://fr.lxcat.net/data/set_type.php).

However, in order to study electron runaway, we have extended the code to 1 keV. Therefore, we have modified the scattering model from an isotropic to an anisotropic algorithm as discussed below, and we have renormalized the elastic momentum transfer cross section according to Li et al. (2012). The cross sections for nitrogen are from Phelps and Pitchford (1985), and the oxygen data are from the Phelps compilation available in the *lxcat data bank*. All collision types with their energy losses are summarized in Table 1, they include attachment, elastic, excitation, and ionization collisions.

We use the empirical fit of Opal et al. (1971) for the distribution of the energy between the two outgoing electrons after an ionization collision. The electron scattering angles after ionization are calculated as by Boeuf and Marode (1982). On the other hand, the scattering angle distribution of elastic and excitation collisions are the same and use the formula derived by Okhrimovskyy et al. (2002) for nitrogen and by Surendra et al. (1990) for oxygen.

2.2. Setup of Simulations

We performed two types of simulations, one in the bulk and one in the flux perspective. The distinction between these different statistical ensembles for reactive plasmas is described for instance in (Blevin & Fletcher, 1984; Li et al., 2012; Robson, 1991). This distinction needs to be made here as well as free electrons appear and disappear during the discharge evolution.

Bulk: We studied an ensemble of electrons under the influence of a range of constant electric fields, that is, we studied them in the bulk perspective (Li et al., 2012) like an experiment does; the composition of the electron ensemble continuously changes as electrons are liberated by impact ionization and disappear due to attachment. The electrons started with vanishing energy, they accelerated initially, and then they converged in time to a stationary electron energy distribution. This analysis focuses on the energy distribution of the whole ensemble and allows to test the predictions of the deterministic friction curve concept.

Flux: Here we started with electrons with an initial energy of 200 eV aligned with the electric field and investigated how they evolved in different electric fields. Focusing on "single" electrons, this analysis is done in the flux perspective (Li et al., 2012), as needed in particle simulations. Differences between the electron behavior in air or pure nitrogen are highlighted by this setup, where we note significant differences in the probability of "tunneling" through the friction curve due to large energy fluctuations (see Figure 2) in combination with electron attachment to oxygen in air.

Both simulation types were performed without geometric boundary, in pure nitrogen or in a mixture of 80% nitrogen and 20% oxygen (artificial air), at a temperature of 273 K and a pressure of 1 bar.

The difference between bulk and flux perspectives highlights a possible source of error, if one does not pay attention on one's statistical framework, since both perspectives are valid in different contexts. The flux perspective is what happens with the individual particle while the bulk perspective shows the collective behavior of the whole particle ensemble.

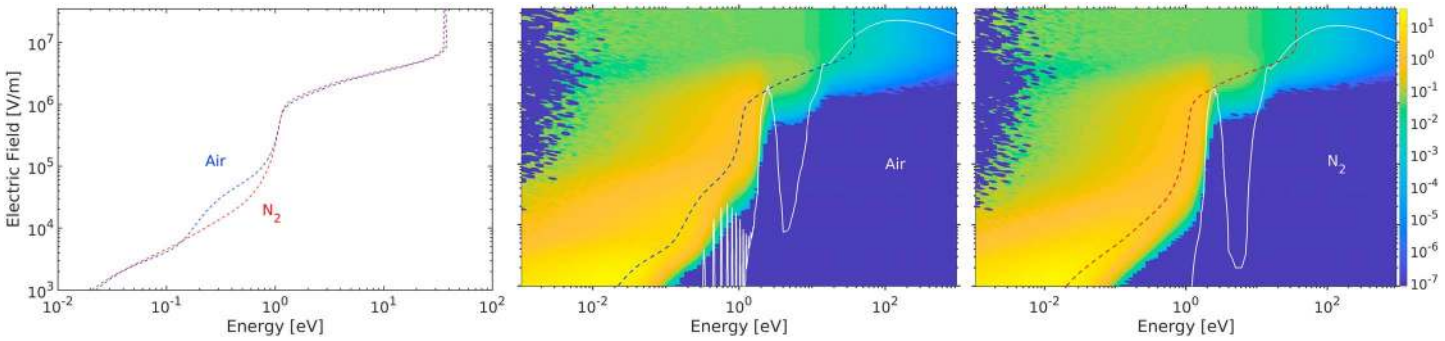

Figure 3. Results of the bulk simulation for the steady state electron energy distributions in constant electric fields ranging from 10^3 to 3.5×10^7 V/m (equivalent to 1 kV/m to 35 MV/m). (left panel) Mean electron energy as a function of the electric field for artificial air (blue) and for pure nitrogen (red). (The electric field is plotted on the *y* axis and applies to all three panels.) (middle panel) Electron energy distribution in air in color coding as a function of the electric field. (right panel) The same as in the middle panel but for pure nitrogen. The color code indicates the electron count per (logarithmic) energy bin, normalized by the total number of particles. The blue or red dashed lines in the middle and the right panels are the mean electron energies that are shown on the left panel as well. The white curves in the middle and the right panels are the respective friction curves from Figure 1 divided by the elementary charge; hence, they have dimension of electric field and can be identified with the equilibrium points of the net force for each electric field, as discussed in the introduction.

2.2.1. Bulk Simulations

The bulk simulations were performed with 10^5 electrons with an initial energy of 0 eV in constant electric fields. The electron number in the ensemble was kept constant by adding an electron at random from the instantaneous electron ensemble after an attachment reaction and by removing a random electron from the ensemble after an ionization reaction; in this way the ensemble averages stay the same, the ensemble develops on its intrinsic time scales, but the particle number stays both numerically manageable and sufficiently large to allow good averaging. We covered the range from 1 kV/m to 35 MV/m of electric fields in order to cover the whole domain of the friction curve represented in Figure 1.

Our energy range is up to 1 keV, and electrons that reach 1 keV in this set up are removed from the simulation and a random particle is added just like after an attachment reaction. Since the energy of the added particle is randomly chosen from the instantaneous distribution, the distribution does not change. However, in high electric fields the ensemble of electrons below 200 eV is strongly coupled to the ensemble with higher energies; therefore, our distribution shows artifacts due to the removal of electrons above 1 keV. This can be seen in Figure 3 where the mean electron energy stops to increase for electric fields above 10 MV/m.

We considered 200 different electric fields values equally spread on a logarithmic scale, and we let the simulations run until the electron ensemble reached steady state. After 4 ns or less we noticed no significant changes of the mean energy and its standard deviation for all electric field values considered. And the standard deviation is always similar to the mean energy, which reflects the broad energy distributions shown in the next section.

2.2.2. Flux Simulations

The flux simulations start with 10^6 electrons with 200 eV energy. The electrons were launched in the direction opposite to the field, so they gain maximal initial acceleration. We let the electrons evolve for 100 ns in constant electric fields between 16 and 34 MV/m. When the electrons reach 1 keV or attach to oxygen, they are flagged and not followed further. When an ionization reaction occurs, the electron with the higher energy is kept, while the other one is removed. In this manner, we focus on those electrons most likely to run away, that is, on those that might tunnel through the friction barrier.

We compute the probability that an electron reaches 1 keV up to time *t*, by accumulating the number of all electrons that reach 1 keV up to that time, divided by the total number of initial electrons. In the same manner, we define the cumulative probability of attachment up to time *t* as the ratio of the total number of attachments up to time *t* over the total number of initial electrons.

Figure 2 shows the particle energy fluctuations in the flux simulation. The energy varies by almost 5 orders of magnitude due to high collision frequency and high electric field. The two different colors in the figure represent two different particles, and we see that one particle disappears after some time due to an attachment collision.

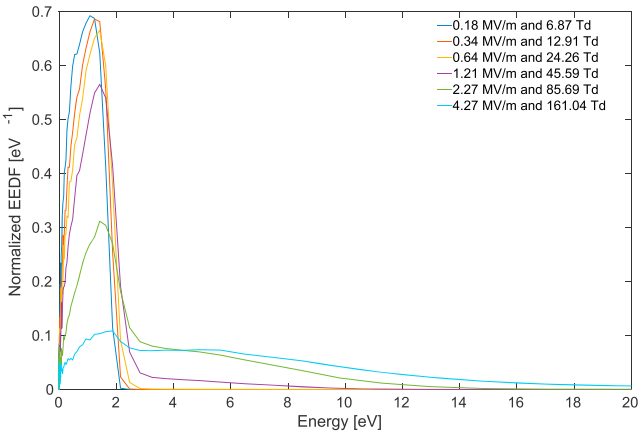

Figure 4. Selected electron energy distributions from Figure 3 for air. The legend displays the electric field in two different units, in MV/m for reference to the present results and in Td for comparison with Colman et al. (2010). EEDF = electron energy distribution function.

3. Results and Discussion

3.1. Steady State Electron Energy Distributions in Different Fields and the Friction Curve

3.1.1. The Electron Energy Distributions

The electron energy distributions in steady state as a function of applied electric field are displayed in Figure 3. To share the same field axis with all three panels, the field is plotted on the *y* axis. It ranges from 1 kV/m to 35 MV/m, which is well above the literature value for the electron runaway threshold of approximately 26 MV/m.

The left panel shows the mean electron energy in artificial air or pure nitrogen as a function of the electric field. The mean electron energy as a function of electric field is essentially the same for pure nitrogen or air, except for mean electron energies between 0.3 and 2 eV, which correspond to electric fields between roughly 10^4 and 10^5 V/m (10 to 100 kV/m). There the mean electron energy in air is lower than in pure nitrogen. This effect can be attributed to electron energy losses due to the excitation of the vibrational states of oxygen, as also visible as the spikes around 1 eV of energy in the friction curve in Figure 1. The mean energy saturates when the electric field approaches 10^7 V/m. This is an artifact of the electron removal at 1 keV.

The middle and right panels show the electron energy distribution in air or nitrogen in color coding as a function of the electric field. The mean energy from the left panel is plotted as a dashed line in the middle and the right panels for the respective gas. Furthermore, the friction curves from Figure 1 are divided by the elementary charge and inserted as a white line in the panels for air or pure nitrogen. We will come back to this curve in the next subsection.

For better visualization of the data in Figure 3, we display the electron energy distributions in air for some selected electric fields between 180 kV/m and 4.27 MV/m in Figure 4. We note that as the electric field increases, the electron energy distribution shifts from a clear maximum below 2 eV to energies above 4 eV. A local minimum of the energy distribution around 3 eV develops in this case that reflects the local maximum of the collisional energy losses due to electronic excitations. A similar observation has been made by Colman et al. (2010).

For electric fields above roughly 3 MV/m, the electron energy distribution is already nonzero up to electron energies of 1 keV. This means that electrons already have a nonvanishing probability to run away in such a field.

3.1.2. The Relation to the Friction Curve

The friction curve from Figure 1 is inserted in the middle and the right panels of Figure 3 as a white line. If it were a systematic approximation, then for each electric field, the intersection of the horizontal line of constant field with the friction curve would define an equilibrium point at this field—as described in section 1. So if friction curve and electric field would fully characterize the electron energy in a deterministic manner, the electron energy distributions should fully collapse onto the friction curves in Figure 3. But obviously that is not the case. And we already have identified the four shortcomings A to D of this approximation in section 1.

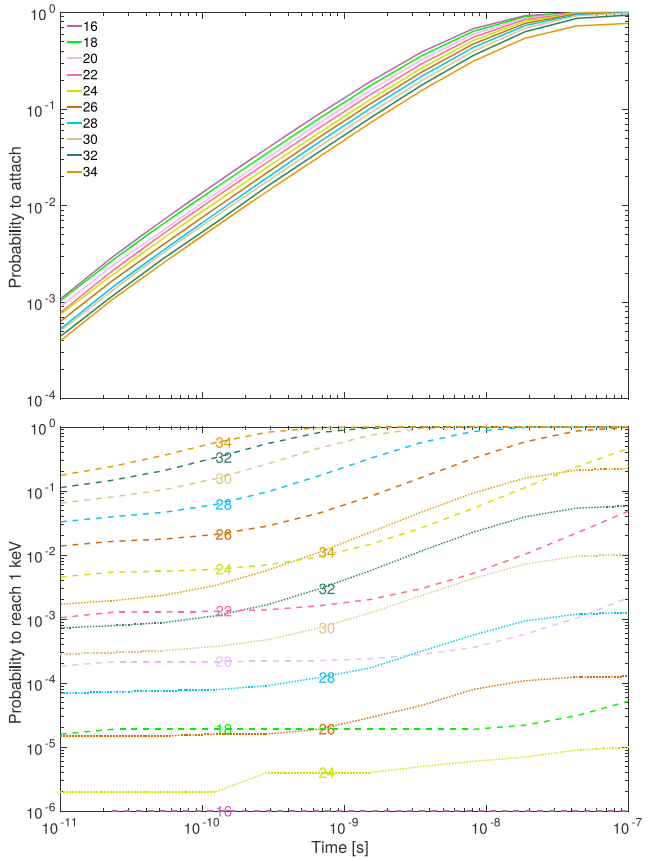

Figure 5. Results of the flux simulation for electrons starting with 200 eV in electric fields from 16 to 34 MV/m where lines of different colors refer to different fields. (top panel) Probability $P(t)$ that an electron in air attaches to oxygen up to time t, as a function of time (for 10 ps to 100 ns). (bottom panel) Probability $P(t)$ that an electron in air (dotted lines) or pure nitrogen (dashed lines) reaches 1 keV, again as a function of field (color coded) and time. The numbers in the plots express the applied electric field in multiples of MV/m.

A further analysis of the middle and right panels of Figure 3 shows the following: For fields up to 10^4 V/m, the friction curve is far above a wide electron energy distribution. For electric fields between 10 kV/m and 1 MV/m, the friction curve in practice seems to mark the upper limit of the electron energy distribution or the energy range where the distribution function decays steeply.

For a large range of electric fields, there are several intersections with the friction curve, that is, a number of equilibrium points. In a purely deterministic setting, one would expect electron energies to be localized at the stable equilibrium points, but that is also not the case. The small dip of the energy distribution at about 3 eV for 4.27 MV/m is a small indication for such behavior.

When there are several stable equilibrium points of the electron energies in a deterministic interpretation, there can be transitions between them. We call this a tunneling effect. (Of course, this tunneling is due to stochastic fluctuations and not to quantum mechanics.) We observe a tunneling process in two different energy and field regimes: first, at the electronic excitation peak at about 2 eV, where the electron energy distributions start to tunnel through the friction curve for electric fields of about 1 MV/m, and second, at the ionization region above 10 eV for electric fields near the classical breakdown value of 3 MV/m.

We finally remark that the electron energy distributions of air and pure nitrogen are quite similar, despite their differences in electron attachment and vibrational excitations.

3.2. Electron Runaway in Electric Fields Below the Runaway Threshold

3.2.1. An Analysis in the Flux Perspective of Single Electrons

We now analyze the probability that an electron reaches the runaway regime as a function of the electric field when it starts out with an energy of 200 eV, and when it is optimally aligned with the electric field. This energy is chosen because the friction at this energy is maximal; see Figure 1. The electrons then have a high collision frequency and large energy losses per collision. The temporal evolution of the energy of two electrons starting with an energy of 200 eV in an electric field of 26 MV/m is shown in Figure 2.

A basic difference between air and pure nitrogen is that electrons in air can attach to oxygen. As they fluctuate through a large range of energies, electrons in air can reach energies where attachment is important, and then they will disappear, as is also illustrated in the right panel of Figure 2. In nitrogen this cannot happen, and the probability that a given electron will run away is much larger.

This effect is quantified in Figure 5. The top panel shows the probability that an electron in air starts with 200 eV and attaches to oxygen up to time t. We can distinguish two different features: First, the probability of attachment reaches almost 100% after 0.1 μs in all electric fields between 16 and 34 MV/m; second, the probability to attach diminishes with increasing electric fields. This is because the mean electron energy gain between collisions increases, and hence, it is less likely that the electron will reach the low energies needed for attachment.

The bottom panel in Figure 5 shows the probability for an electron with initial 200 eV to reach 1 keV up to time t while it moves through air (dotted curves) or pure nitrogen (dashed curves). The colors of the lines indicate electric fields from 16 to 34 MV/m. Since nitrogen does not have attachment reactions, there is no sink mechanism for the electrons in the simulation, except that they are removed from the sample when they reach 1 keV, while electrons in air attach massively. Therefore, single electrons in pure nitrogen reach 1 keV after maximally 100 ns with a probability of 50% in a field of 24 MV/m, while single electrons in air need more than 34 MV/m for a runaway probability above 50%. In a field of 18 MV/m, single electrons in pure nitrogen

already reach 1 keV within 100 ns with a probability of about 10^{-4}, while in air they would need a field of 25 MV/m.

3.2.2. The Bulk Perspective on the Electron Ensemble

From the above analysis one might conclude that electron runaway is largely suppressed in an electronegative gas where electrons can attach. However, this is what happens in the flux perspective that focused on the energy evolution of single electrons.

The energy fluctuations shown in Figure 2 indicate that electrons with initial energies as high as 200 eV play no very distinctive role in electron runaway, as they typically first explore a large range of lower energies before possibly running away.

In fact, Figure 3 clearly indicates that the electron energy distribution stretches to 1 keV for electric fields above 3 MV/m. This is the fact both for air and for pure nitrogen. The energy distribution of the whole electron ensemble is established collectively by all collision processes including electron loss due to attachment and electron gain due to impact ionization, and no major difference between air or pure nitrogen can be seen.

4. Conclusion

We have performed two different types of Monte Carlo simulations, both in pure nitrogen and in artificial air. In the bulk simulations, we have calculated the electron energy distributions of a dynamically changing electron ensemble in a wide range of electric fields. We have found that electrons can reach energies of 1 keV (which was the upper limit of the energies we explored) already in a field of about 3 MV/m, which is the classical breakdown field.

We also have compared our results with predictions from the friction curve as calculated by Moss et al. (2006). In section 1, we have already discussed that friction is a valid concept at high (relativistic) energies, but that there are shortcomings when applied below 1 keV: in particular, the nonalignment of electron motion and electric field, due to the random electron scattering directions after electron molecule collisions is not taken into account; also, the energy loss is not a continuous friction process but happens in discrete stochastic events. And the dynamic change of the electron ensemble cannot be included either. For this reason, the friction curve in the energy range below 1 keV does not characterize the mean electron energies in a given electric field, but in practice it rather seems to act like the upper bound of a very broad electron energy distribution. Where the friction curve would predict the coexistence of two stable electron energies, the stochastic electron ensemble tunnels through the curve and creates a broad distribution. For the same reason, the maximum of the friction curve of 24 MeV/m is not a strict threshold to runaway, but electrons can reach energies of 1 keV in fields of as low as 3 MV/m.

In a second Monte Carlo simulation, we have calculated the probability that a single electron starting with 200 eV reaches 1 keV or is being attached, in a range of electric fields. Here attachment is a major factor, and one might conclude that electron runaway below fields of 24 MV/m is suppressed by attachment in air but not in pure nitrogen. However, this single electron (or flux) perspective does not represent the behavior of the whole reactive electron ensemble in the ensemble (or bulk) perspective of the first Monte Carlo experiment, as discussed above. This first experiment shows that the electron ensemble can tunnel through the friction curve for electric fields well below the runaway threshold, in a similar manner in air and in pure nitrogen.

Acknowledgments

U. E. thanks Jannis Teunissen for first indicating that the definition (1) of the friction curve requires an alignment of electric field and electron trajectory. G. D. and I. F. acknowledge financial support by CAPES, CNPq, and FAPDF, and G. D. and C. R. also acknowledge funding by FOM project 12PR3041. The data are displayed in the article, and the code can be accessed at https://github.com/jannisteunissen/particle_core/tree/anisotropic-mod/src.

References

Adachi, T., Takahashi, Y., Ohya, H., Tsuchiya, F., Yamashita, K., Yamamoto, M., & Hashiguchi, H. (2008). Monitoring of lightning activity in Southeast Asia: Scientific objectives and strategies. Kyoto Working Papers on Area Studies: G-COE Series.

Babich, L. P., Bochkov, E. I., Kutsyk, I. M., & Roussel-Dupré, R. A. (2010). Localization of the source of terrestrial neutron bursts detected in thunderstorm atmosphere. *Journal of Geophysical Research*, *115*, A00E28. https://doi.org/10.1029/2009JA014750

Babich, L., Donskoy, E., Kutsyk, I., & Roussel-Dupré, R. (2005). The feedback mechanism of runaway air breakdown. *Geophysical Research Letters*, *32*, L09809. https://doi.org/10.1029/2004GL021744

Bakhov, K. I., Babich, L. P., & Kutsyk, I. M. (2000). Temporal characteristics of runaway electrons in electron-neutral collision-dominated plasma of dense gases. Monte Carlo calculations. *IEEE Transactions on Plasma Science*, *28*(4), 1254–1262. https://doi.org/10.1109/27.893314

Blevin, H. A., & Fletcher, J. (1984). Transport and rate coefficients in townsend discharges. *Australian Journal of Physics*, *37*, 593–600. https://doi.org/10.1071/PH840593

Boeuf, J. P., & Marode, E. (1982). A Monte Carlo analysis of an electron swarm in a non-uniform field: The cathode region of a glow discharge in helium. *Journal of Physics D: Applied Physics*, *15*(11), 2169–2187.

Bowers, G. S., Smith, D. M., Martinez-McKinney, G., Kamogawa, M., Cummer, S., Dwyer, J., et al. (2017). Gamma ray signatures of neutrons from a terrestrial gamma ray flash. *Geophysical Research Letters*, *44*, 10,063–10,070. https://doi.org/10.1002/2017GL075071

Briggs, M. S., Connaughton, V., Wilson-Hodge, C., Preece, R. D., Fishman, G. J., Kippen, R. M., et al. (2011). Electron-positron beams from terrestrial lightning observed with Fermi GBM. *Geophysical Research Letters*, *38*, L02808. https://doi.org/10.1029/2010GL046259

Chanrion, O., Bonaventura, Z., Bourdon, A., & Neubert, T. (2016). Influence of the angular scattering of electrons on the runaway threshold in air. *Plasma Physics and Controlled Fusion*, *58*(4), 044001.

Chanrion, O., Bonaventura, Z., Çinar, D., Bourdon, A., & Neubert, T. (2014). Runaway electrons from a "beam-bulk" model of streamer: Application to TGFs. *Environmental Research Letters*, *9*(5), 055003.

Chilingarian, A., Daryan, A., Arakelyan, K., Hovhannisyan, A., Mailyan, B., Melkumyan, L., et al. (2010). Ground-based observations of thunderstorm-correlated fluxes of high-energy electrons, gamma rays, and neutrons. *Physical Review D*, *82*(4), 043009. https://doi.org/10.1103/PhysRevD.82.043009

Chilingarian, A., Hovsepyan, G., & Hovhannisyan, A. (2011). Particle bursts from thunderclouds: Natural particle accelerators above our heads. *Physical Review D*, *83*(6), 062001. https://doi.org/10.1103/PhysRevD.83.062001

Colman, J. J., Roussel-Dupré, R. A., & Triplett, L. (2010). Temporally self-similar electron distribution functions in atmospheric breakdown: The thermal runaway regime. *Journal of Geophysical Research*, *115*, A00E16. https://doi.org/10.1029/2009JA014509

Dubinova, A., Rutjes, C., Ebert, U., Buitink, S., Scholten, O., & Trinh, G. T. N. (2015). Prediction of lightning inception by large ice particles and extensive air showers. *Physical Review Letters*, *115*(1), 015002. https://doi.org/10.1103/PhysRevLett.115.015002

Dwyer, J. R. (2004). Implications of x-ray emission from lightning. *Geophysical Research Letters*, *31*, L12102. https://doi.org/10.1029/2004GL019795

Dwyer, J. R. (2007). Relativistic breakdown in planetary atmospheres. *Physics of Plasmas*, *14*(4), 042901. https://doi.org/10.1063/1.2709652

Dwyer, J., Saleh, Z., Rassoul, H., Concha, D., Rahman, M., Cooray, V., et al. (2008). A study of x-ray emission from laboratory sparks in air at atmospheric pressure. *Journal of Geophysical Research*, *113*, D23207. https://doi.org/10.1029/2008JD010315

Enoto, T., Wada, Y., Furuta, Y., Nakazawa, K., Yuasa, T., Okuda, K., et al. (2017). Photonuclear reactions triggered by lightning discharge. *Nature*, *551*, 481.

Fishman, G. J., Bhat, P. N., Mallozzi, R., Horack, J. M., Koshut, T., Kouveliotou, C., et al. (1994). Discovery of intense gamma-ray flashes of atmospheric origin. *Science*, *264*, 1313–1316. https://doi.org/10.1126/science.264.5163.1313

Gurevich, A., Milikh, G., & Roussel-Dupre, R. (1992). Runaway electron mechanism of air breakdown and preconditioning during a thunderstorm. *Physics Letters A*, *165*(5), 463–468. https://doi.org/10.1016/0375-9601(92)90348-P

International Commission on Radiation Units and Measurements (1984). Stopping powers of electrons and positrons, ICRU Rep. 37, Bethesda, Md.

Li, C., Ebert, U., & Hundsdorfer, W. (2009). 3D hybrid computations for streamer discharges and production of runaway electrons. *Journal of Physics D: Applied Physics*, *42*(20), 202003.

Li, C., Ebert, U., & Hundsdorfer, W. (2012). Spatially hybrid computations for streamer discharges: II. Fully 3D simulations. *Journal of Computational Physics*, *231*(3), 1020–1050. https://doi.org/10.1016/j.jcp.2011.07.023

Moss, G. D., Pasko, V. P., Liu, N., & Veronis, G. (2006). Monte carlo model for analysis of thermal runaway electrons in streamer tips in transient luminous events and streamer zones of lightning leaders. *Journal of Geophysical Research*, *111*, A02307. https://doi.org/10.1029/2005JA011350

Okhrimovskyy, A., Bogaerts, A., & Gijbels, R. (2002). Electron anisotropic scattering in gases: A formula for Monte Carlo simulations. *Physical Review E*, *65*, 037402. https://doi.org/10.1103/PhysRevE.65.037402

Opal, C. B., Peterson, W. K., & Beaty, E. C. (1971). Measurements of secondary electron spectra produced by electron impact ionization of a number of simple gases. *The Journal of Chemical Physics*, *55*(8), 4100–4106. https://doi.org/10.1063/1.1676707

Østgaard, N., Gjesteland, T., Stadsnes, J., Connell, P., & Carlson, B. (2008). Production altitude and time delays of the terrestrial gamma flashes: Revisiting the burst and transient source experiment spectra. *Journal of Geophysical Research*, *113*, A02307. https://doi.org/10.1029/2007JA012618

Phelps, A. V., & Pitchford, L. C. (1985). Anisotropic scattering of electrons by N_2 and its effect on electron transport. *Physical Review A*, *31*, 2932–2949. https://doi.org/10.1103/PhysRevA.31.2932

Robson, R. E. (1991). Transport phenomena in the presence of reactions: Definition and measurement of transport coefficients. *Australian Journal of Physics*, *44*, 685–692. https://doi.org/10.1071/PH910685

Rutjes, C., Diniz, G., Ferreira, I. S., & Ebert, U. (2017). TGF afterglows: A new radiation mechanism from thunderstorms. *Geophysical Research Letters*, *44*, 10,702–10,712. https://doi.org/10.1002/2017GL075552

Rutjes, C., Sarria, D., Skeltved, A. B., Luque, A., Diniz, G., Østgaard, N., & Ebert, U. (2016). Evaluation of Monte Carlo tools for high energy atmospheric physics. *Geoscientific Model Development*, *9*(11), 3961–3974. https://doi.org/10.5194/gmd-9-3961-2016

Skeltved, A. B., Østgaard, N., Carlson, B., Gjesteland, T., & Celestin, S. (2014). Modeling the relativistic runaway electron avalanche and the feedback mechanism with GEANT4. *Journal of Geophysical Research: Space Physics*, *119*, 9174–9191. https://doi.org/10.1002/2014JA020504

Surendra, M., Graves, D. B., & Jellum, G. M. (1990). Self-consistent model of a direct-current glow discharge: Treatment of fast electrons. *Physical Review A*, *41*, 1112–1125. https://doi.org/10.1103/PhysRevA.41.1112

Teunissen, J., & Ebert, U. (2016). 3D PIC-MCC simulations of discharge inception around a sharp anode in nitrogen/oxygen mixtures. *Plasma Sources Science and Technology*, *25*, 044005.

Tsuchiya, H., Enoto, T., Yamada, S., Yuasa, T., Kawaharada, M., Kitaguchi, T., et al. (2007). Detection of high-energy gamma rays from winter thunderclouds. *Physical Review Letters*, *165002*(16). https://doi.org/10.1103/PhysRevLett.99.165002

Wilson, C. (1924). The electric field of a thundercloud and some of its effects. *Proceedings of the Physical Society of London*, *37*(1), 32D.